

This work was written as part of one of the author's official duties as an Employee of the United States Government and is therefore a work of the United States Government. In accordance with 17 U.S.C. 105, no copyright protection is available for such works under U.S. Law.

Public Domain Mark 1.0

<https://creativecommons.org/publicdomain/mark/1.0/>

Access to this work was provided by the University of Maryland, Baltimore County (UMBC) ScholarWorks@UMBC digital repository on the Maryland Shared Open Access (MD-SOAR) platform.

Please provide feedback

Please support the ScholarWorks@UMBC repository by emailing scholarworks-group@umbc.edu and telling us what having access to this work means to you and why it's important to you. Thank you.

Direct auroral precipitation from the magnetotail during substorms

Maha Ashour-Abdalla,^{1,2} David Schriver,^{1,2} Mostafa El Alaoui,^{1,2} Robert Richard,^{1,2} Raymond Walker,^{1,3,4} Melvyn L. Goldstein,⁵ Eric Donovan,⁶ and Meng Zhou⁷

Received 16 May 2013; accepted 4 June 2013; published 30 July 2013.

[1] In this study, we examine the causes of electron precipitation during a substorm on 15 February 2008 that lead to auroral brightening. We use global kinetic simulations along with spacecraft and ground-based data. We find \sim keV electrons in the region modeled in the simulation precipitate into the premidnight sector at latitudes between 71° and 75° due to two distinct physical processes: (1) higher latitude precipitation due to electrons that undergo relatively rapid non-adiabatic pitch angle scattering into the loss cone just earthward of a reconnection region, and (2) lower latitude precipitation due to electrons that are more gradually accelerated primarily parallel to the geomagnetic field by Fermi acceleration. These latter electrons enter the loss cone much closer to Earth at ~ -15 to $-10 R_E$. The electron precipitation due to the combination of these two mechanisms coincides spatially with observed auroral brightening during the disturbed event. **Citation:** Ashour-Abdalla, M., D. Schriver, M. E. Alaoui, R. Richard, R. Walker, M. L. Goldstein, E. Donovan, and M. Zhou (2013), Direct auroral precipitation from the magnetotail during substorms, *Geophys. Res. Lett.*, 40, 3787–3792, doi:10.1002/grl.50635.

1. Introduction

[2] The visible aurora at high latitudes provides a window on dynamic plasma processes that occur in the Earth's magnetosphere. Although most researchers agree that particle flow, field-aligned currents, and electromagnetic fields from the magnetotail drive auroral dynamics, a direct connection between processes in the magnetotail at -25 to $-10 R_E$ and the low altitude auroral zone is still the subject of intense research. Theories suggested to explain auroral dynamics involve large scale parallel electric fields, double layers, solitary structures, Alfvén waves and various types of wave-particle interactions [Borovsky, 1993]

[3] It has been known for some time that field-aligned precipitating electrons with keV energies cause discrete aurora [e.g., McIlwain, 1960; Hoffman and Evans, 1968; Frank and Ackerson, 1971] and it is a reasonable hypothesis that such electron precipitation ultimately results from processes occurring in the magnetotail [e.g., Frank, 1985; Lyons *et al.*, 1999]. The basic idea is that there is a transfer of energy in the form of earthward-propagating currents, particles, and waves that originate in the magnetotail into field-aligned accelerated electrons in the auroral zone. It is well established that quasi-static (dc) parallel electric fields (inverted V structures and parallel potential drops) occur in regions of field-aligned current [Mozer *et al.*, 1977; Elphic *et al.*, 1998; Ergun *et al.*, 2000; Nakamura *et al.*, 2001; Kepko *et al.*, 2009]. While small scale auroral structure is probably related to low altitude processes, the broader scale distribution of auroral precipitation is governed by field-aligned currents systems from the magnetotail [e.g., Haerendel, 1989]. The existence of a magnetotail driver for kinetic Alfvén wave auroral acceleration is supported by observations of intense Poynting flux detected in a region above, but magnetically connected to the discrete auroral precipitation region [Wygant *et al.*, 2000; Keiling *et al.*, 2001].

[4] In this paper, we present a scenario for auroral precipitation during disturbed times in which keV electrons are scattered into the loss cone in the magnetotail current sheet relatively far from Earth, i.e., $-10 > x > -25 R_E$ (using Geocentric Solar Magnetospheric coordinates). We analyze a substorm event observed on 15 February 2008 that featured enhanced auroral brightening and earthward-propagating dipolarization fronts from magnetotail reconnection [Zhou *et al.*, 2009; Ashour-Abdalla *et al.*, 2011]. Using large scale kinetic electron particle tracing within a global magnetohydrodynamic (MHD) model of this event, we show that precipitating \sim keV electrons between about 71° and 75° latitude in the premidnight sector map directly to a relatively wide region of the magnetotail current sheet. These electrons enter the loss cone due to two distinctly different physical processes occurring at different magnetotail locations. Earthward of the reconnection region ($-25 < x < -20 R_E$), we find electrons that started with relatively large pitch angles (well outside the loss cone) experience non-adiabatic motion when passing through the sharply bent current sheet field lines and are stochastically pitch angle scattered into the loss cone [Zelenyi *et al.*, 1990]. These precipitate into the ionosphere in the premidnight sector in the upper part of the latitude range. At lower latitudes adiabatic Fermi acceleration leads to the direct precipitation of electrons from the magnetotail. These precipitating electrons start at $x \sim -20 R_E$ with small pitch angles ($\sim 10^\circ$), outside of the loss cone, and have fairly long mirror bounce paths. Convection transports these electrons earthward with each

¹Institute of Geophysics and Planetary Physics, UCLA, Los Angeles, California, USA.

²Department of Physics and Astronomy, UCLA, Los Angeles, California, USA.

³Department of Earth and Space Sciences, UCLA, Los Angeles, California, USA.

⁴National Science Foundation, Arlington, Virginia, USA.

⁵Heliospheric Physics Laboratory, NASA Goddard Space Flight Center, Greenbelt, Maryland, USA.

⁶Department of Physics and Astronomy, University of Calgary, Calgary, Alberta, Canada.

⁷Institute of Space Science and Technology, Nanchang University, Nanchang, China.

Corresponding author: M. Ashour-Abdalla, Institute of Geophysics and Planetary Physics, UCLA, 405 Hilgard Ave., 3860 Slichter Hall, Los Angeles, CA 90095-1567, USA. (mabdalla@igpp.ucla.edu)

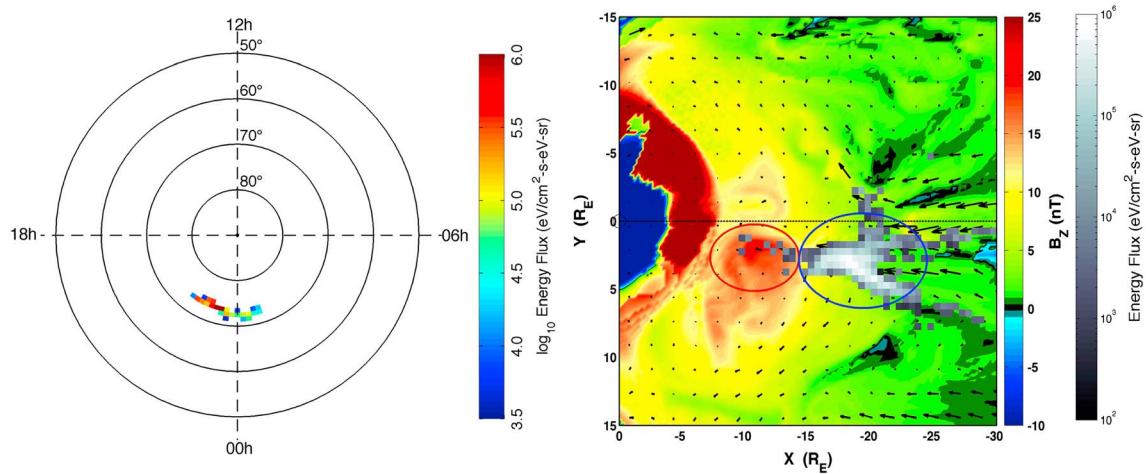


Figure 1. (left) Precipitating electron flux at 100 km altitude is shown in a latitude-local time polar display with each circle representing 10° increments in latitude (90° at the center) color coded in energy flux with units $\text{eV}/\text{cm}^2 \text{ s eV sr}$. (right) Shown are the locations of the last crossings of the precipitating electrons in the magnetotail maximum pressure plane binned in $0.5 R_E$ by $0.5 R_E$ boxes as indicated by the white-gray scale squares with white corresponding to a peak energy flux of $10^6 \text{ eV}/\text{cm}^2 \text{ s eV sr}$. Both panels are shown at 03:58:00 UT. Two dynamically distinct classes of particles are distinguished by red and blue ovals in Figure 1 (right).

bounce through the current sheet. Conservation of the second adiabatic invariant ($I = \int p_{\parallel} ds$, where the parallel momentum p_{\parallel} is integrated along the path length s over a mirror bounce) leads to a gradual increase in parallel energy. The pitch angle gradually decreases until the electron enters the loss cone earthward of $x \sim -15 R_E$ and precipitates. The two types of electron precipitation occur at locations in general agreement with ground-based all-sky camera observations of auroral brightening.

[5] In section 2 of this paper, we describe the substorm event on 15 February 2008 and the simulation model. In section 3, we present the simulation results and compare them to all-sky camera images. Section 4 contains the summary and conclusions.

2. Substorm Event Characteristics and Simulation Model

[6] We consider a well documented geomagnetic substorm event that occurred on 15 February 2008 in which multiple earthward-propagating dipolarization fronts were observed by different THEMIS satellites [Zhou *et al.*, 2009; Ashour-Abdalla *et al.*, 2011] grouped in the near-Earth tail near the equator ($z \sim 0$) between $x = -12$ and $-8 R_E$, and $y \sim 2 R_E$. During the substorm expansion phase, THEMIS P4 detected two dipolarization fronts: one at 03:57:00 UT and another at 03:57:38 UT. The dipolarization fronts were characterized by rapid increases in B_z and by an increased flux of energetic electrons at 30 keV to 207 keV, whereas the flux of the thermal energy plasma ($< 30 \text{ keV}$) decreased. Fluxes in the two highest energy channels (297 keV and 427 keV) did not change. All-sky images from different stations at high northern latitudes showed auroral brightening premidnight at latitudes near 73° starting at about 03:55:00 UT.

[7] This event was modeled by using a global MHD simulation [El-Alaoui 2001] driven by observed upstream solar wind conditions, which reproduced the earthward-propagating dipolarization fronts observed by THEMIS [Ashour-Abdalla *et al.*, 2011]. Since MHD simulations

approximate the plasma as a single ion-dominated fluid, electron kinetic effects are not included, thus to study electron particle dynamics in the magnetotail we used the large scale kinetic (LSK) technique. In the LSK simulations, a large number of charged particle trajectories are followed in the time-dependent electric and magnetic fields obtained from the MHD simulations [Ashour-Abdalla *et al.*, 1997; Birn *et al.*, 1998; 2004]. The electron trajectories are followed by using a method that switches between full particle and guiding center equations of motion where the local conditions determine which set of motion equations to use [Schrifer *et al.* 2011; Birn *et al.*, 2004]. We carried out an electron launch scheme similar to Ashour-Abdalla *et al.* [2011] and launched 10^5 particles every 20 s from 03:47:00 UT to 03:58:00 UT (total 3.30×10^7 particles). A Maxwellian distribution ($T = 1 \text{ keV}$) was launched in the plasma sheet earthward of the neutral line between $x = -17$ to $-21 R_E$, $y = -1.0$ to $-4.5 R_E$, $z = -3.5 R_E$. The launch location is earthward of the reconnection site ($-35 R_E$ to $-25 R_E$). Reconnection occurred continuously until the end of the run (04:00:00 UT) though the rate and location varied. Our previous studies examined the high energy enhancement in the near-Earth plasma sheet associated with the dipolarization front [Ashour-Abdalla *et al.*, 2011; Pan *et al.*, 2012]. The focus here is on electrons that are lost from the magnetotail and precipitate into the ionosphere. In the LSK simulations, electrons are considered as precipitating if they reached the inner boundary of the global MHD simulation, which is a spherical surface at $2.8 R_E$ from the center of the Earth. The precipitation profiles are then created by mapping these electrons to 100 km altitude along dipole field lines where they interact with the ionosphere to create auroral light.

3. Auroral Precipitation: Simulation and Data Results

[8] Results from the LSK simulations of the precipitating electrons at 03:58:00 UT are shown in Figure 1, with the location of precipitating electron energy flux on a polar plot in Figure 1 (left) and the locations where the corresponding

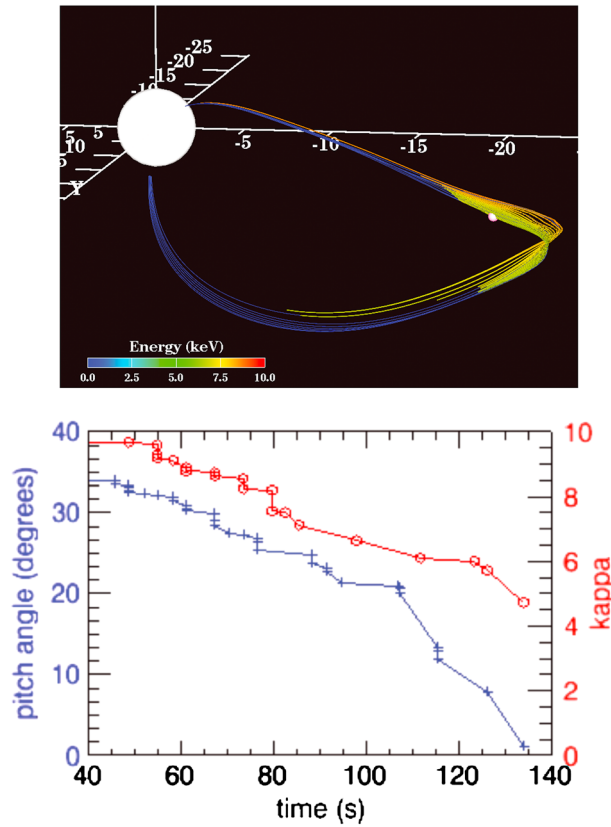


Figure 2. (top) The trajectory of an electron experiencing non-adiabatic stochastic pitch angle scattering is shown. (bottom) The lower envelopes of time histories of the pitch angle in blue (scale on left) and kappa parameter in red are displayed (scale on right), where $\kappa = (R/\rho)^{1/2}$.

particles last crossed the maximum pressure surface before precipitating in Figure 1 (right). The precipitating electrons in Figure 1 (right) were mapped back to their last crossing of the maximum pressure surface with the energy flux shown on a gray scale. The electron crossing locations are superimposed on color contours of the MHD magnetic field B_z component and arrows that show the MHD bulk plasma flow direction at 03:58:00 UT. The precipitating electrons were found to originate from regions in the equatorial magnetosphere indicated by the red and blue regions circled in Figure 1 (right).

[9] The results show a region of electron precipitation in the premidnight sector between about 71° and 75° geomagnetic latitude with peak energy flux of 10^6 eV/cm²s eV sr and average particle energy of 5–10 keV (Figure 1, left). The precipitating electrons crossed the maximum pressure plane between about $-25 R_E$ and $-10 R_E$ (Figure 1, right), which is earthward of the reconnection region, but tailward of the dipolarization front observed at 03:57:00 UT by THEMIS P4. The red and blue circles in Figure 1 differentiate two physical mechanisms that cause electrons to precipitate into the ionosphere. The electrons enclosed by the blue circle precipitate from the deeper magnetotail at $\sim -25 R_E$ to $-15 R_E$ due to non-adiabatic stochastic pitch angle scattering [Zelenyi *et al.*, 1990]. Figure 2 (top) shows a three-dimensional electron trajectory while Figure 2 (bottom) shows the time history of pitch angle (blue) and particle

κ (red). The kappa parameter is defined as the square root of the radius of magnetic field curvature R divided by the gyroradius ρ , i.e., $\kappa = (R/\rho)^{1/2}$ at the local position of the particle [Büchner and Zelenyi, 1986]. Kappa is a measure of a particle's adiabaticity, with smaller values, i.e., $\kappa < 5$ indicating that its motion can be quasi- or non-adiabatic without a well defined gyro-center [Büchner and Zelenyi, 1986; Delcourt *et al.*, 1995]. In general, if $\kappa > 10$, the particle motion is highly adiabatic and follows guiding center equations of motion [Northrop, 1963]. Both traces give the values as the particle crosses the equatorial current sheet and both show a decreasing trend. The electron trajectory (Figure 2, top) is sharply kinked at the current sheet crossings, indicating the smaller magnetic field curvature radius there. The electron initially has a relatively large pitch angle $>45^\circ$ (Figure 2, bottom) and thus it has a relatively short bounce path between magnetic mirror points. Kappa is about 10 at this time, but as the electron drifts in y to a region of weaker equatorial magnetic field, κ decreases and on subsequent current sheet crossings stochastic pitch angle scattering occurs, further decreasing the pitch angle. By the time κ decreases to <5 , the pitch angle has been scattered to $<1^\circ$, at which point it is within the loss cone and the electron precipitates. This occurs $\sim 22 R_E$ downtail and the particle precipitates into the ionosphere at $\sim 74^\circ$ latitude. In general non-adiabatic pitch angle scattering can either increase or decrease the pitch angle and only a few percent of the launched electrons experienced a decrease in pitch angle such that they precipitated. Non-adiabatic electrons whose overall pitch angles increased remained in the system and contributed to the heated central plasma sheet [Ashour-Abdalla *et al.*, 2011].

[10] Precipitating electrons that enter the loss cone closer to the Earth, i.e., $> -15 R_E$ as circled in red on Figure 1, behave very differently. One such electron is illustrated in Figure 3. The three-dimensional trajectory is in Figure 3 (top), the time history of the second adiabatic invariant I , path length s , and pitch angle are in Figure 3 (middle), and the time history of the log of the particle energy (total, parallel, and perpendicular) is in Figure 3 (bottom). This particle initially started near the neutral line earthward of $-20 R_E$. It has a relatively small pitch angle to begin with ($\sim 8^\circ$) and has a long bounce path between mirror points that are relatively close to the Earth (Figure 3, top). Even near the neutral line, it did not pass through a region where κ became small. Particle motion is highly adiabatic with $\kappa > 50$ (not shown). The second invariant of motion I , defined as the parallel momentum integrated over a bounce path, i.e., $I = \int p_{\parallel} ds$, is well conserved. As the electron convects earthward, it moves onto shorter field lines and the path length decreases (Figure 3, middle), causing the parallel momentum to increase. The parallel energy increases gradually with time due to Fermi acceleration (Figure 3, bottom), which when coupled with a relatively small increase in the perpendicular energy due to betatron acceleration results in an ever decreasing pitch angle. As the particle continues its bounce motion, its pitch angle continues to decrease and it will eventually enter the loss cone earthward of $-12 R_E$ causing precipitation at relatively lower latitudes ($<72^\circ$) than the non-adiabatically scattered particle. Note the loss cone gets wider closer to the Earth allowing particles with larger pitch angles to precipitate.

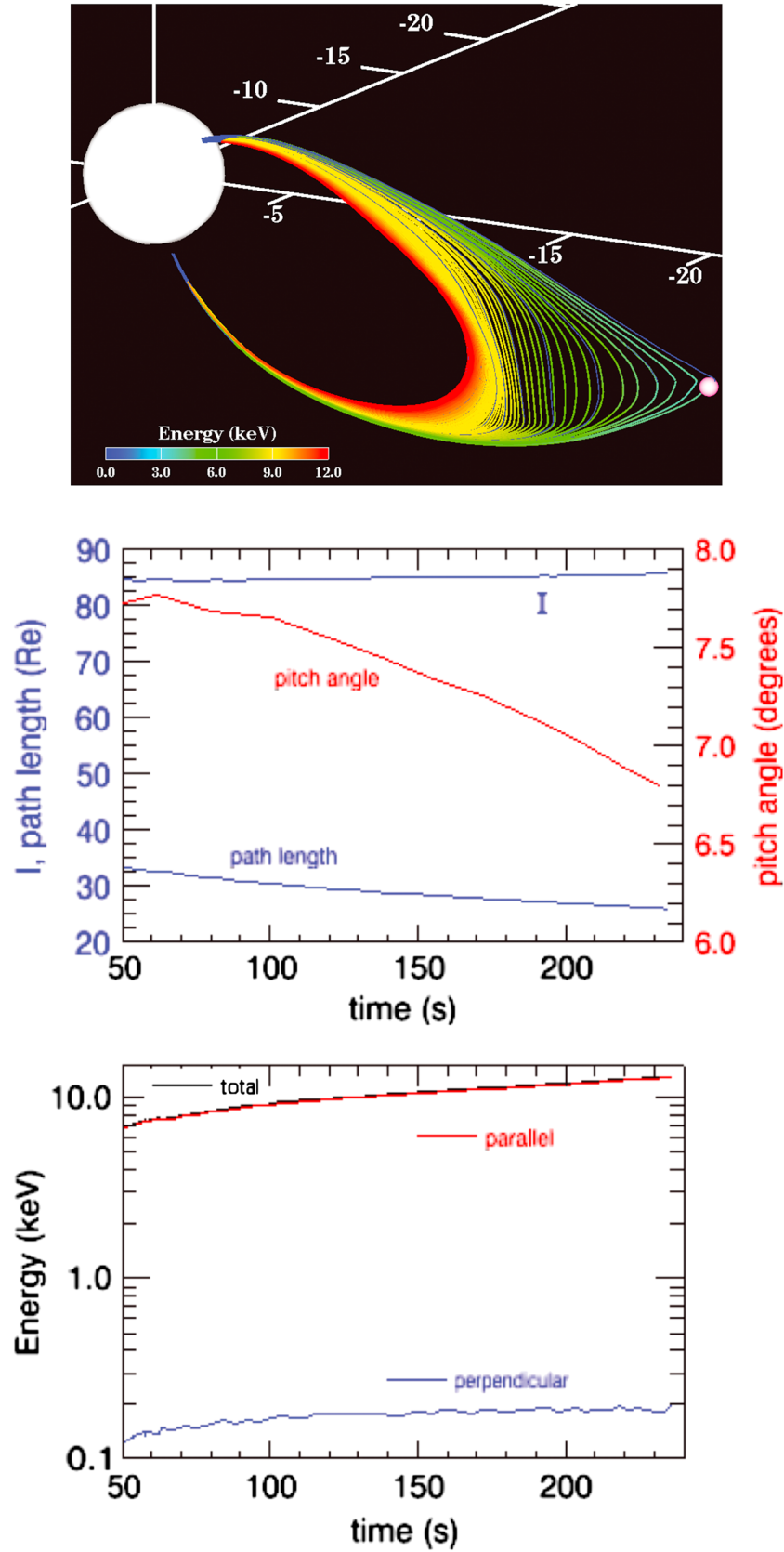


Figure 3. (top) The trajectory of a Fermi accelerated particle is shown. (middle) The time history of the second adiabatic invariant ($I = \int p_{\parallel} ds$ shown by the black trace), the bounce path length in blue (scale in R_E on the left), and pitch angle (in degrees) in red (scale on the right) are shown. (bottom) The time history of the components of the particle energy (total in black, parallel in red, perpendicular in blue) is shown.

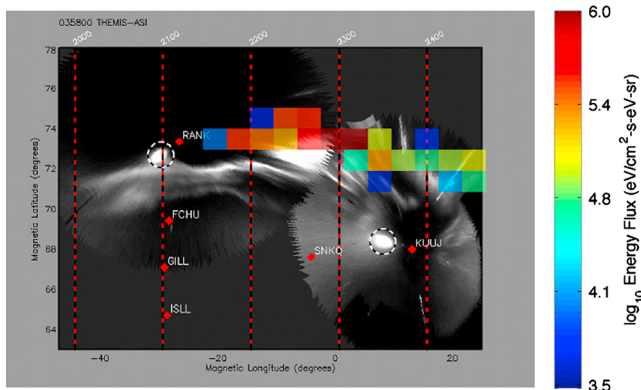


Figure 4. Images from the Kuujuaq and Rankin Inlet THEMIS-ASIs from 03:58:00 UT on 15 February 2008. The images are plotted in geomagnetic coordinates and we have assumed an emission height of 100 km. The vertical red dashed lines indicate magnetic local times. The white dashed circles indicate the moon as seen from the two imagers. Precipitating electron fluxes from the simulations (see text) are plotted over the images.

[11] The locations found from the simulations for all of the electrons that precipitate show good correspondence in latitude and local time with the auroral brightening during the substorm event. This is illustrated in Figure 4, which is a composite in magnetic coordinates of two all-sky images from THEMIS-ASI stations [see, e.g., *Donovan et al., 2006; Mende et al., 2008*] at 03:58:00 UT. Superimposed on the all-sky images are the locations of the precipitating electrons from the simulation. The electrons at lower latitudes tend to be Fermi accelerated, and those at higher latitudes are primarily ones that were stochastically pitch angle scattered. There is a good correlation between the location of the precipitating electrons and an auroral brightening seen at RANK (Rankin Inlet) and at KUUI (Kuujuaq) stations just before midnight (note that the bright spot circled in the all-sky images is the Moon). Based on the auroral images in the minutes leading up to the auroral brightening, there was an auroral arc structure spanning at least 4 h of MLT (2000–2400). Starting at about 03:55:00 UT, the auroral brightening began in the 2200–2400 MLT sector. The auroral brightening continued and evolved into the tilted streamers evident in Figure 4. These streamers extend roughly 4° equatorward from the latitude of the preexisting arc. Starting from 03:54:00 UT, the simulation results showed that there was enhancement in the precipitating electron energy flux with a peak at about 03:59:00 UT in qualitative agreement with the observed auroral brightening. These results suggest that the mechanisms described here that lead to auroral brightening during the substorm expansion phase may be different from the physical processes that lead to the quiet time auroral arc electron precipitation occurring prior to the expansion phase.

4. Discussion and Summary

[12] During this substorm, earthward-propagating dipolarization fronts were observed by THEMIS spacecraft in the near-Earth magnetotail plasma sheet and auroral brightening was observed by all-sky cameras at high northern latitudes around 70° in the premidnight sector. Previous kinetic simulations for

this event have shown that electrons can be accelerated to ~ 100 keV within the dipolarization front in the plasma sheet by a combination of non-adiabatic acceleration near the magnetotail reconnection region and adiabatic betatron acceleration within the dipolarization front. This acceleration can account for the enhancement in energetic electrons observed when the dipolarization front passes over the THEMIS spacecraft [Ashour-Abdalla et al., 2011].

[13] While some of the electrons are strongly energized during this event, they primarily have large pitch angles [Ashour-Abdalla et al., 2011], while it is seen here that electrons with more modest energies (\sim keV) can have smaller pitch angles and precipitate into the ionosphere. Two acceleration mechanisms cause electrons to enter the loss cone from the magnetotail in the simulation. For both types, the average precipitating energy is about 5–10 keV and the energy flux is $\sim 10^5$ eV/cm²s eV sr. The first acceleration mechanism leading to precipitation is stochastic pitch angle scattering that occurs at about 20–25 R_E downtail where the magnetic field is relatively weak and particles can be non-adiabatic. Some of these non-adiabatic electrons are scattered into the loss cone reducing the fluxes of these lower energy (\sim keV) electrons in the plasma sheet. The electron shown in Figure 2 was adiabatic until the last three bounces, became non-adiabatic when it entered the current sheet and then was transported earthward. The second acceleration mechanism is Fermi acceleration, which causes adiabatic electrons to enter the loss cone closer to the Earth between about $-10 R_E$ and $-15 R_E$. THEMIS observations near $-10 R_E$ in the magnetotail show a dropout in lower energy (5–10 keV) electrons after the dipolarization front passes the satellite and the electrons in this energy range are observed to have low pitch angles (more field-aligned). This is consistent with our results which show that the low pitch angle electrons tend to precipitate tailward of $-10 R_E$ due to the combined non-adiabatic and Fermi acceleration processes, leaving a relatively few of these particles in the plasma sheet. In contrast, betatron acceleration leads to an enhancement of flux at larger pitch angles and at energies up to 100 keV as found in Ashour-Abdalla et al. [2011].

[14] These two types of motion combine to form a precipitation pattern in the ionosphere in the premidnight sector between about 71° and 75° . To the precision of our simulation, the location, timing, and energy of these precipitating electrons are in good agreement with all-sky camera images of auroral brightening at substorm onset. The results here imply that auroral emissions can be caused by a number of mechanisms. Quiet time auroral arcs are likely to be caused by a combination of low altitude ($<10,000$ km) field-aligned electron acceleration processes that result in electron precipitation, including double layers, inverted V structures, inertial Alfvén waves, and wave-particle interactions. At lower latitudes that map to the Earth's radiation belt region $<9 R_E$, wave-particle interactions due to electron cyclotron harmonic waves and whistler-chorus emissions can result in diffuse auroral precipitation [Kennel, 1969] and low altitude electron microbursts [Lorentzen et al., 2001]. The results here show that mechanisms that operate in the magnetotail current sheet between $-10 R_E$ and $-25 R_E$ also can lead to electron precipitation and auroral brightening during substorms. Ultimately all of these different processes result in the visually beautiful aurora.

[15] **Acknowledgments.** Research at UCLA was supported by the NASA MMS Interdisciplinary Science Program grant NNX08AO48G, NASA grant NNX12AD13G, NASA-GI NX10AQ47G, NSF GEM grant AGS-1203739 and NSF AGS-1241405. RJW was on leave at NSF and this work was supported by the NSF Independent Research and Development program. MLG was supported in part by the MMS IDS program at Goddard Space Flight Center. We acknowledge NASA contract NAS5-02099 and V. Angelopoulos for use of data from the THEMIS Mission. Computing was carried out on NASA Advanced Supercomputing and NSF XSEDE platforms.

[16] The Editor thanks Joachim Birn and an anonymous reviewer for their assistance in evaluating this paper.

References

- Ashour-Abdalla, M., et al. (1997), Ion sources and acceleration mechanisms inferred from local distribution functions, *Geophys. Res. Lett.*, **24**(8), 955–958, doi:10.1029/97GL00060.
- Ashour-Abdalla, M., M. El-Alaoui, M. L. Goldstein, M. Zhou, D. Schriver, R. Richard, R. J. Walker, M. G. Kivelson, and K.-J. Hwang (2011), Observations and simulations of non-local acceleration of electrons in magnetotail magnetic reconnection events, *Nature*, **7**, 360–365, doi:10.1038/nphys1903.
- Birn, J., M. F. Thomsen, J. E. Borovsky, G. D. Reeves, D. J. McComas, R. D. Belian, and M. Hesse (1998), Substorm electron injections: Geosynchronous observations and test particle simulations, *J. Geophys. Res.*, **103**(A5), 9235–9248, doi:10.1029/97JA02635.
- Birn, J., M. F. Thomsen, and M. Hesse (2004), Electron acceleration in the dynamic magnetotail: Test particle orbits in three-dimensional magneto-hydrodynamic simulation fields, *Phys. Plasmas*, **11**, 1825–1833.
- Borovsky, J. E. (1993), Auroral arc thicknesses as predicted by various theories, *J. Geophys. Res.*, **98**(A4), 6101–6138, doi:10.1029/92JA02242.
- Büchner, J., and L. M. Zelenyi (1986), Deterministic chaos in the dynamics of charged-particles near a magnetic-field reversal, *Phys. Lett. A*, **118**, 395–399, doi:10.1016/0375-9601(86)90268-9.
- Delcourt, D. C., J. A. Sauvaud, R. F. Martin, and T. E. Moore (1995), Gyrophase effects in the centrifugal impulse model of particle motion in the magnetotail, *J. Geophys. Res.*, **100**, 17,211–17,220, doi:10.1029/95JA00657.
- Donovan, E., et al. (2006), The THEMIS all-sky imaging array: System design and initial results from the prototype imager, *J. Atmos. Sol. Terr. Phys.*, **68**, 1472–1487.
- El-Alaoui, M. (2001), Current disruption during November 24, 1996, substorm, *J. Geophys. Res.*, **106**(A4), 6229–6245, doi:10.1029/1999JA000260.
- Elphic, R. C., et al. (1998), The auroral current circuit and field aligned currents observed by FAST, *Geophys. Res. Lett.*, **25**(12), 2033–2036, doi:10.1029/98GL01158.
- Ergun, R. E., C. W. Carlson, J. P. McFadden, F. S. Mozer, and R. J. Strangeway (2000), Parallel electric fields in discrete arcs, *Geophys. Res. Lett.*, **27**(24), 4053–4056, doi:10.1029/2000GL003819.
- Frank, L. A. (1985), Plasmas in the earth's magnetotail, *Space Sci. Rev.*, **42**, 211–240, doi:10.1007/BF00218233.
- Frank, L. A., and K. L. Ackerson (1971), Observation of charged particle precipitation into the auroral zone, *J. Geophys. Res.*, **76**(16), 3612–3643.
- Haerendel, G. (1989), Cosmic linear accelerators, in *Proceedings of an International School and Workshop on Plasma Astrophysics*, edited by T. D. Guyenne, and J. J. Hunt, *Eur. Space Agency Spec. Publ.*, **ESA SP-285**, 37–44.
- Hoffman, R. A., and D. S. Evans (1968), Field-aligned electron bursts at high latitude observed by Ogo 4, *J. Geophys. Res.*, **73**(19), 6201–6214.
- Keiling, A., J. R. Wygant, C. Cattell, K.-H. Kim, C. T. Russell, D. K. Milling, M. Temerin, F. S. Mozer, and C. A. Kletzing (2001), Pi2 pulsations observed with the Polar satellite and ground stations: Coupling of trapped and propagating fast mode waves to a midlatitude field line resonance, *J. Geophys. Res.*, **106**(A11), 25,891–25,904, doi:10.1029/2001JA900082.
- Kennel, C. F. (1969), Consequences of a magnetospheric plasma, *Rev. Geophys.*, **7**, 379–419, doi:10.1029/RG007i001p00379.
- Kepko, L., E. Spanswick, V. Angelopoulos, E. Donovan, J. McFadden, K.-H. Glassmeier, J. Raeder, and H. J. Singer (2009), Equatorward moving auroral signatures of a flow burst observed prior to auroral onset, *Geophys. Res. Lett.*, **36**, L24104, doi:10.1029/2009GL041476.
- Lorentzen, K. R., J. B. Blake, U. S. Inan, and J. Bortnik (2001), Observations of relativistic electron microbursts in association with VLF chorus, *J. Geophys. Res.*, **106**(A4), 6017–6027, doi:10.1029/2000JA003018.
- Lyons, L. R., H. E. J. Koskinen, J. B. Blake, A. Egeland, M. Hirahara, M. Oieroset, P. E. Sandholt, and K. Shiokawa (1999), Processes leading to plasma losses into the high-latitude atmosphere, *Space Sci. Rev.*, **88**, 85–135, doi:10.1023/A:1005251700516.
- McIlwain, C. E. (1960), Direct measurements of particles producing visible auroras, *J. Geophys. Res.*, **65**(9), 2727–2747.
- Mende, S., S. Harris, H. Frey, V. Angelopoulos, E. Donovan, B. Jackel, M. Greffen, C. Russell, and L. Peticolas (2008), The THEMIS array of ground based observatories for the study of substorms, *Space Sci. Rev.*, **141**, 357–387.
- Mozer, F. S., C. W. Carlson, M. K. Hudson, R. B. Torbert, B. Parady, J. Yatteau, and M. C. Kelley (1977), Observations of paired electrostatic shocks in polar magnetosphere, *Phys. Rev. Lett.*, **38**, 292–295, doi:10.1103/PhysRevLett.38.292.
- Nakamura, K., W. Baumjohann, R. Schodel, M. Brittnacher, V. A. Sergeev, M. Kubyshkina, T. Mukai, and K. Liou (2001), Earthward flow bursts, auroral streamers, and small expansions, *J. Geophys. Res.*, **106**(A6), 10,791–10,802, doi:10.1029/2000JA000306.
- Northrop, T. G., (1963), *The Adiabatic Motion of Charged Particles*, John Wiley, New York.
- Pan, Q., M. Ashour-Abdalla, M. El-Alaoui, R. J. Walker, and M. L. Goldstein (2012), Adiabatic acceleration of suprathermal electrons associated with dipolarization fronts, *J. Geophys. Res.*, **117**, A12224, doi:10.1029/2012JA018156.
- Schriver, D., et al. (2011), Electron transport and precipitation at Mercury during the MESSENGER flybys: Implications for electron-stimulated desorption, *Planet. Space Sci.*, **59**, 2026–2036, doi:10.1016/j.pss.2011.03.008.
- Wygant, J. R., et al. (2000), Polar spacecraft based comparisons of intense electric fields and Poynting flux near and within the plasma sheet-tail lobe boundary to UVI images: An energy source for the aurora, *J. Geophys. Res.*, **105**(A8), 18,675–18,692, doi:10.1029/1999JA900500.
- Zelenyi, L., A. Galeev, and C. F. Kennel (1990), Ion precipitation from the inner plasma sheet due to stochastic diffusion, *J. Geophys. Res.*, **95**(A4), 3871–3882, doi:10.1029/JA095iA04p03871.
- Zhou, M., M. Ashour-Abdalla, X. Deng, D. Schriver, M. El-Alaoui, and Y. Pang (2009), THEMIS observation of multiple dipolarization fronts and associated wave characteristics in the near-Earth magnetotail, *Geophys. Res. Lett.*, **36**, L20107, doi:10.1029/2009GL040663.